

This is the accepted manuscript made available via CHORUS. The article has been published as:

### Developing the math

$$S \left( \frac{p}{d} \right)^{32} \left( \frac{p}{\gamma} \right)^{31}$$
 reaction to probe the math

$$P \left( \frac{p}{\gamma} \right)^{30} \left( \frac{p}{\gamma} \right)^{31}$$
 reaction rate in classical novae

S. Burcher, K. A. Chipps, R. O. Hughes, C. S. Reingold, A. Saastamoinen, J. T. Harke, N. Cooper, S. Ahn, J. M. Allmond, H. Clark, J. A. Cizewski, M. R. Hall, J. Hooker, H. Jayatissa, K. L. Jones, S. Ota, S. D. Pain, K. Schmidt, A. Simon, and S. Upadhyayula

DOI: [10.1103/PhysRevC.105.045805](https://doi.org/10.1103/PhysRevC.105.045805)

# Developing the $^{32}\text{S}(p,d)^{31}\text{S}^*(p)(\gamma)$ Reaction to Probe the $^{30}\text{P}(p,\gamma)^{31}\text{S}$ Reaction Rate in Classical Novae

S. Burcher,<sup>1,2</sup> K.A. Chipps,<sup>3,1,\*</sup> R.O. Hughes,<sup>2</sup> C.S. Reingold,<sup>4,†</sup> A. Saastamoinen,<sup>5</sup> J.T. Harke,<sup>2</sup> N. Cooper,<sup>4,‡</sup> S. Ahn,<sup>5</sup> J.M. Allmond,<sup>3</sup> H. Clark,<sup>5</sup> J.A. Cizewski,<sup>6</sup> M.R. Hall,<sup>3</sup> J. Hooker,<sup>5</sup> H. Jayatissa,<sup>5</sup> K.L. Jones,<sup>1</sup> S. Ota,<sup>5</sup> S.D. Pain,<sup>3</sup> K. Schmidt,<sup>7,8,§</sup> A. Simon,<sup>4</sup> and S. Upadhyayula<sup>5</sup>

<sup>1</sup>*Department of Physics and Astronomy, University of Tennessee, Knoxville, Tennessee 37996, USA*

<sup>2</sup>*Physics Division, Lawrence Livermore National Laboratory, Livermore, California 94551, USA*

<sup>3</sup>*Physics Division, Oak Ridge National Laboratory, Oak Ridge, Tennessee 37831, USA*

<sup>4</sup>*Department of Physics, University of Notre Dame, Notre Dame, Indiana 46556, USA*

<sup>5</sup>*Texas A&M Cyclotron Institute, College Station, Texas 77840, USA*

<sup>6</sup>*Department of Physics and Astronomy, Rutgers University, New Brunswick, New Jersey 08903, USA*

<sup>7</sup>*National Superconducting Cyclotron Laboratory, Michigan State University, East Lansing, Michigan 48824, USA*

<sup>8</sup>*Joint Institute for Nuclear Astrophysics - Center for the Evolution of the Elements, East Lansing, Michigan 48824, USA*

(Dated: April 13, 2022)

**Background:** The  $^{30}\text{P}(p,\gamma)^{31}\text{S}$  reaction rate is one of the largest remaining sources of uncertainty in the final abundances of nuclei created in a classical nova involving a ONe white dwarf. The reaction rate directly influences silicon isotopic ratios which are used as identifiers of pre-solar grains with nova origins. In addition, the uncertainty in the  $^{30}\text{P}(p,\gamma)^{31}\text{S}$  reaction rate has been found to limit the use of nova nuclear thermometers based on observations of elemental ratios in nova ejecta.

**Purpose:** Reduce uncertainties in the nuclear data for proton-unbound states in  $^{31}\text{S}$  which act as resonances for the  $^{30}\text{P}(p,\gamma)^{31}\text{S}$  reaction at classical nova temperatures, and develop a technique for high efficiency, high resolution reaction-decay coincidence measurements.

**Methods:** The  $^{32}\text{S}(p,d)^{31}\text{S}$  reaction was used to populate the states of interest in  $^{31}\text{S}$ . The experiment was performed at the Texas A&M Cyclotron Institute using the LLNL Hyperion array for the detection of charged particles and  $\gamma$  rays. A downstream silicon telescope was used to select reaction deuterons, and a single upstream silicon detector was used to measure protons emitted in the decay of unbound  $^{31}\text{S}$  levels.

**Results:** Several states in  $^{31}\text{S}$  above the proton separation energy were observed to have been populated. Decay protons from the resonant states in  $^{31}\text{S}$  were identified as events in the upstream silicon detectors that came in coincidence with deuterons in the downstream telescope. Protons emitted from these states were measured and branching ratios extracted.

**Conclusion:** While no new reaction rate is derived, spin-parity assignments for several higher-lying proton unbound states have been confirmed. Measured  $p_0$  branching ratios for these levels have been compared to previous measurements with good agreement, and in some cases provided a reduction in uncertainty. The previously identified  $T = 3/2$  state may have been incorrectly assigned a large  $p_0$  branching ratio in a previous measurement. The technique of measuring reaction-decay coincidences with a particle-gamma setup appears promising.

## I. INTRODUCTION

Classical novae are explosive nuclear burning events that occur in binary star systems consisting of a white dwarf and lesser evolved main-sequence star. Some of the material generated in such an event will be ejected from the surface of the white dwarf into the interstellar medium, enriching it with isotopes synthesized in the nova. Nucleosynthesis in a classical nova occurs via a series of proton-capture reactions and  $\beta^+$  decays. The nuclei present in the white dwarf act as seeds for the series

of proton-capture reactions, and therefore the composition of the white dwarf plays a crucial role in the final abundance of nuclei produced in a nova [1]. Oxygen-neon (ONe) novae occur on the heaviest of white dwarfs. The relatively heavier nuclei present in ONe white dwarfs, and the high peak temperature of ONe nova, ranging from 0.1 to 0.4 GK [2], allow for the synthesis of nuclei up to the intermediate mass region ( $A \approx 40$ ) [1].

Despite these conditions in ONe novae, the  $^{30}\text{P}(p,\gamma)^{31}\text{S}$  reaction acts as a bottleneck for nucleosynthesis beyond  $A = 30$ . The region of the nuclear chart around  $^{30}\text{P}$  is shown in Figure 1 with nucleosynthetic pathways labeled by arrows. The bottleneck at  $A = 30$  is due, in part, to the relatively long  $\beta^+$ -decay half life of  $^{30}\text{P}$  ( $t_{1/2} = 2.5$  minutes) compared to the time-scale of the thermonuclear runaway in a nova event, which is on the order of hundreds of seconds. Once  $^{30}\text{P}$  is created, the primary path for nucleosynthesis to proceed to higher mass is via the  $^{30}\text{P}(p,\gamma)^{31}\text{S}$  reaction, making

\* Corresponding author

† Current address: Physics Division, Lawrence Livermore National Laboratory, Livermore, California 94551, USA

‡ Deceased

§ Present Address: Institute of Radiation Physics, Helmholtz-Zentrum Dresden-Rossendorf, Bautzner Landstrasse 400, 01328 Dresden, Germany

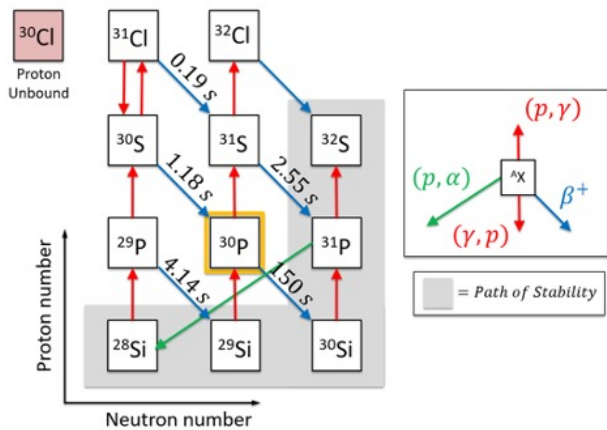


FIG. 1: (Color online) The region of the nuclear chart around  $^{30}\text{P}$  with some of the reactions important for ONe nova nucleosynthesis labeled. The values displayed above the blue diagonal lines are the  $\beta^+$ -decay half lives. Figure reproduced from Ref. [3].

the final abundances of nuclei with  $A \gtrsim 30$  particularly sensitive to the  $^{30}\text{P}(p, \gamma)^{31}\text{S}$  reaction rate. More proton-rich paths to higher mass are inhibited by the low proton binding energy of  $^{31}\text{Cl}$ , which makes the competing photo-dissociation reaction favorable even at classical nova temperatures.

Some of the nuclei whose abundances are influenced by the  $^{30}\text{P}(p, \gamma)^{31}\text{S}$  reaction rate are important for key nova observables, such as presolar grain analysis [4, 5] and the spectroscopy of nova ejecta [6, 7]. Presolar grains are identified by isotopic ratios that differ from those found in the majority of matter in our solar system, indicative of an origin pre-dating the formation of our solar system. The definitive identification of grains from an ONe nova is currently limited by uncertainties in some of the key nuclear reaction rates involved in ONe nova nucleosynthesis [5].

The isotopic ratio of  $^{30}\text{Si}/^{28}\text{Si}$  in presolar grains has been identified as a potential signature of ONe nova origin and can also be used to determine the peak temperature of a nova [5]. The  $^{30}\text{P}(p, \gamma)^{31}\text{S}$  reaction rate directly affects the  $^{30}\text{Si}$  abundance as it is produced through the  $\beta^+$  decay of  $^{30}\text{P}$ , which is in direct competition with proton capture on  $^{30}\text{P}$ . The effect of the  $^{30}\text{P}(p, \gamma)^{31}\text{S}$  reaction rate on the final abundance of  $^{30}\text{Si}$  for different peak-temperature nova models [8] is shown in Figure 2. The final abundance of  $^{30}\text{Si}$  shows a strong monotonic dependence on the  $^{30}\text{P}(p, \gamma)^{31}\text{S}$  reaction rate, whereas the final abundance of  $^{28}\text{Si}$  is not affected by the  $^{30}\text{P}(p, \gamma)^{31}\text{S}$  reaction rate. Therefore, the variation in the  $^{30}\text{Si}/^{28}\text{Si}$  isotopic ratio due to the  $^{30}\text{P}(p, \gamma)^{31}\text{S}$  reaction rate scales with the final abundance of  $^{30}\text{Si}$ . Presently, however, the uncertainty in the  $^{30}\text{P}(p, \gamma)^{31}\text{S}$  reaction rate inhibits the use of the  $^{30}\text{Si}/^{28}\text{Si}$  isotopic ratio as a signature of ONe nova origin of some presolar grains [5].

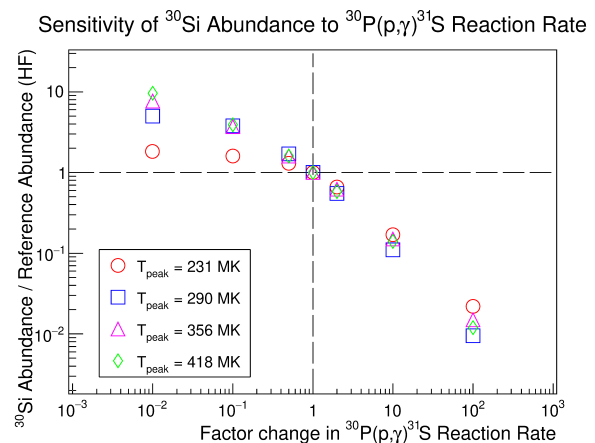


FIG. 2: (Color online) The sensitivity of  $^{30}\text{Si}$  abundance to the  $^{30}\text{P}(p, \gamma)^{31}\text{S}$  reaction rate for different peak ONE nova temperatures. The dashed lines correspond to the reaction rate derived from the Hauser-Feshbach (HF) statistical method and the resulting  $^{30}\text{Si}$  abundance.

The data presented here have been extracted from Tables 5,6,7, and 8 in Ref. [8].

The  $^{30}\text{P}(p, \gamma)^{31}\text{S}$  reaction rate at classical nova temperatures remains poorly constrained experimentally, despite recent efforts to probe the reaction via indirect techniques. To calculate the reaction rate, the cross section must be known across the energy range of interest, with the temperatures involved corresponding to center of mass energies of approximately 100 to 500 keV. Early attempts to calculate the  $^{30}\text{P}(p, \gamma)^{31}\text{S}$  cross section as a function of energy employed the Hauser-Feshbach (HF) statistical method [9]; however, the nuclear level density in  $^{31}\text{S}$ , at the relevant excitation energies for classical nova temperatures, is likely to be insufficiently high for the HF method to yield accurate results. The cross section can be more accurately calculated by considering the contributions from individual resonances, for which basic nuclear structure information, such as the excitation (resonance) energy, spin and parity, lifetime, and partial widths. Use of an alternate reaction to probe each or several of these properties for the levels in  $^{31}\text{S}$  relevant to the  $^{30}\text{P}(p, \gamma)^{31}\text{S}$  capture cross section can help to provide a more experimentally-constrained reaction rate.

Gamma spectroscopy, either from fusion evaporation (e.g. [10, 11]) or single-nucleon transfer (e.g. [12]), have proven powerful tools to determine the resonance energies and spins of unbound levels in  $^{31}\text{S}$  with high precision. Particle spectroscopy (e.g. [13, 14]) also provides level energy and  $J^\pi$  information, and can be used to probe higher-lying resonances, for which the gamma branch becomes diminishingly small. Utilizing a particle spectroscopy approach combined with the detection of particle decays from populated unbound levels in  $^{31}\text{S}$  in coincidence, such as in Ref. [15], additionally provides experimental constraint on the particle branching ratios of the populated levels. Because the  $\beta$ -decay of

$^{31}\text{Cl}$  populates many of the levels in  $^{31}\text{S}$  important to the  $^{30}\text{P}(p, \gamma)^{31}\text{S}$  reaction rate, the use of  $\beta$ -delayed  $\gamma$  spectroscopy [16, 17] can also provide a mechanism for studying the energy and spin information of these states. Combining this technique with the simultaneous detection of decay protons from the  $^{31}\text{S}$  unbound levels [18] allows for the extraction of proton branching ratios, which, when combined with a measurement of the level lifetime or total width, experimentally constrains the resonance strengths critical to our understanding of the  $^{30}\text{P}(p, \gamma)^{31}\text{S}$  reaction [19].

Hence, it is apparent that experimental techniques which can simultaneously constrain multiple properties of the levels involved represent the largest return-on-investment for such an indirect study, and provide important nuclear structure information which can be used to benchmark theoretical calculations and guide future direct measurements. In the current work, particle spectroscopy using a single-nucleon transfer reaction was combined with coincident measurements of gamma rays and protons emitted from the populated unbound levels in an attempt to constrain both the proton and gamma branching ratios simultaneously. While the current work was unable to reliably extrapolate such data from  $^{31}\text{S}$  levels within the relevant energy range, the measurement acts as a proof-of-principle for future work seeking to better constrain the  $^{30}\text{P}(p, \gamma)^{31}\text{S}$  reaction rate.

## II. EXPERIMENT

The  $^{32}\text{S}(p, d)^{31}\text{S}$  reaction was chosen to populate the proton-unbound states in  $^{31}\text{S}$  which may contribute to the  $^{30}\text{P}(p, \gamma)^{31}\text{S}$  reaction at ONe nova temperatures. Following the population of excited states in  $^{31}\text{S}$ , the competition between proton and  $\gamma$ -ray emission was observed.

The Texas A&M Cyclotron Institute's K150 cyclotron was used to accelerate a proton beam to 33.0(1) MeV onto the reaction target. The beam current was measured by a Faraday cup at the beam dump, located several meters downstream of the target chamber and shielded to reduce beam-induced  $\gamma$ -ray background. The beam current ranged from 0.5-1.8 nA throughout the experiment and was adjusted, depending on the thickness of the target, to maintain  $\approx 80\%$  livetime in the data acquisition system. The main target used for the experiment was ZnS ( $178 \mu\text{g}/\text{cm}^2$ ) deposited on a thin carbon backing ( $5 \mu\text{g}/\text{cm}^2$ ). In addition, data were taken with carbon, zinc, and mylar ( $\text{C}_{10}\text{H}_8\text{O}_4$ ) $_n$  targets for detector calibrations and background characterization.

The Hyperion Array [20] was used to measure charged particles and  $\gamma$  rays resulting from interactions of the beam with the target. In the configuration used for this experiment, Hyperion consisted of 12 Compton-suppressed high-purity germanium (HPGe) clover detectors, a silicon telescope downstream of the target, and a single silicon detector upstream of the target. All of the silicon detectors used in this experiment were standard

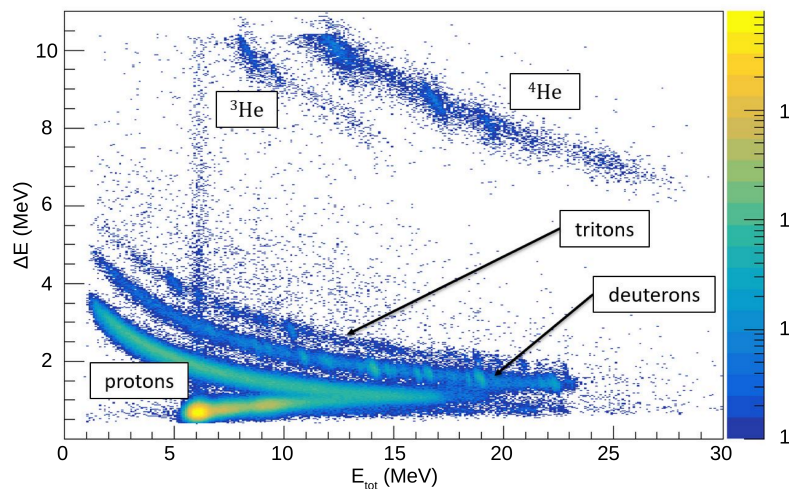


FIG. 3: (Color online) An example of a  $\Delta E$ - $E$  particle identification plot. The data shown here are for a scattering angle of  $20^\circ$  and were taken over one hour. Scattered protons, deuterons, tritons,  $^3\text{He}$ , and  $^4\text{He}$ , produced in the corresponding proton-induced reactions on nuclei in the target, are visible and well separated. The intensity, ranging from single counts (blue/dark grey) to thousands of counts (yellow/light grey) per bin, has not been normalized.

Micron Semiconductor S2 design [21], and were segmented with 24 annular strips, each with 1 mm pitch, on the junction side and eight  $45^\circ$  sectors on the Ohmic side. The silicon detectors were calibrated with a  $^{226}\text{Ra}$   $\alpha$  source, followed by a secondary calibration using known, strongly-populated levels in the (p,d) reactions on the various targets. The  $\Delta E$  and  $E$  detectors of the telescope were positioned 28 mm downstream of the target, covered an angular range of  $20$ - $50^\circ$  in the lab, and were  $150 \mu\text{m}$  and  $1500 \mu\text{m}$  thick respectively. The silicon telescope was used for particle identification and provided a clean gate on deuterons produced in the  $^{32}\text{S}(p, d)^{31}\text{S}$  reaction as shown in Figure 3. The angular segmentation of the telescope allowed for the measurement of the scattering (polar) angle of the charged particles with an angular resolution of  $\approx 1$  degree in the laboratory frame. A single  $500 \mu\text{m}$  thick silicon detector was placed 34 mm upstream of the target and was used for the detection of protons emitted from proton-unbound states in  $^{31}\text{S}$ . This configuration of charged-particle detectors, summarized in Table I, allowed for the detection of reaction-decay coincidences across an angular range of  $90$ - $180^\circ$  between the two particles. The data acquisition system master trigger required an event in both the  $\Delta E$  and  $E$  detectors of the silicon telescope. Events measured by the upstream silicon detector and HPGe clovers that came in coincidence with  $\Delta E$ - $E$  events, within a  $5 \mu\text{s}$  gate, were recorded.

The  $\gamma$ -ray detection efficiency was measured using multiple standard sources of known activity ( $^{152}\text{Eu}$ ,  $^{137}\text{Cs}$ , and  $^{60}\text{Co}$ ) placed at the target location. The effi-

TABLE I: List of the charged particle detectors used in the Hyperion setup for this measurement. 12 of the 14 HPGe clovers in the standard formation were utilized in the current work. For additional details, the reader is directed to Ref. [20].

Detector type, description	Det. thickness ( $\mu\text{m}$ )	Location	Angular range (degrees, lab)
Micron S2, E layer	1500	28mm, downstream	20-50
Micron S2, $\Delta E$ layer	150	28mm, downstream	20-50
Micron S2, decay protons	500	34mm, upstream	17-43

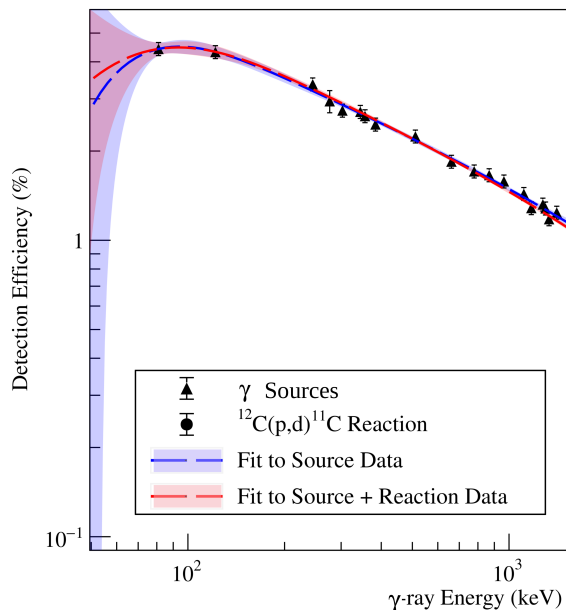


FIG. 4: (Color online) Gamma-ray detection efficiency curve. Fits for source data only (blue/light grey outer band) and source data plus in-beam data (red/dark grey inner band) are shown, with the corresponding uncertainties. Including both source and in-beam data allows for more accurate extrapolation to higher gamma-ray energies.

ciency was then fit using Eq. 1

$$\varepsilon(E_\gamma) = c_0 + c_1 E_\gamma^{-c_2} - c_3 e^{-c_4 E_\gamma} \quad (1)$$

The  $\gamma$ -ray sources available for calibration were limited to  $\gamma$ -ray energies  $\lesssim 1.4$  MeV. However,  $\gamma$  rays up to 6-7 MeV were expected in the experiment. The fit to the measured source efficiency was extrapolated to the higher energies. To verify the validity of the extrapolation,  $\gamma$  rays from the de-excitation of  $^{11}\text{C}$ , following the  $^{12}\text{C}(p, d)^{11}\text{C}$  reaction were used. The efficiency measured in the beam-on, reaction setting was found to be in good agreement with the extrapolation of the fit to source data, as shown in Figure 4.

TABLE II: Optical Model and neutron bound state parameters used for the DWBA analysis. The three rows are for the incoming proton channel, the outgoing deuteron channel and the binding potential of the transferred neutron in  $^{32}\text{S}$ . The proton parameters were obtained from Kozub et al. [13] and the deuteron parameters from Cowley et al. [22].

	$r_c$ (fm)	$V_0$ (MeV)	$r_0$ (fm)	$a_0$ (fm)	$V_i$ (MeV)	$r_i$ (fm)	$a_i$ (fm)
$p$	1.18	47.1	1.18	0.66	6.87	1.18	0.66
$d$	1.18	90.0	1.25	0.62	25.0	1.30	0.58
$n$			1.20	0.65			

### III. ANALYSIS

Deuteron spectra are generated by gating on the PID plot and using the known 2-body kinematics to convert the measured energy and angle of the deuteron into  $^{31}\text{S}$  excitation energy. Figure 5 shows the deuteron singles spectrum, for all angles, from the main experimental target in black, with normalized deuteron spectra from the mylar and zinc foils in blue and red respectively. By comparing these spectra it is possible to identify deuteron peaks that are the result of the  $^{32}\text{S}(p, d)^{31}\text{S}$  reaction and reject structures that are arising from reactions on other nuclei in the target. Peaks corresponding to the population of states in  $^{31}\text{S}$  with excitation energies above the proton separation energy were identified in the spectra at each laboratory angle and fit using a Gaussian (or sum of Gaussians) of set width along with a linear background term. Some example angular distributions are plotted in Figure 6. In some cases contaminant peaks, due to the stoichiometric components of the target material (mainly carbon; reactions on the zinc did not populate discrete levels) or due to environmental contamination (such as nitrogen) were not able to be resolved from peaks of interest. However, due to the differing kinematics, these peaks did not interfere at all angles. Angles at which the separation of the peaks was clear were used to inform the intensity of the interfering peaks at angles where the two peaks could not be resolved. This was possible because the angular distributions of the contaminant peaks were measured with the carbon and mylar (nitrogen-rich) targets and used to constrain their intensity when they were unable to be resolved from the peak of interest.

The deuteron angular distributions for states above the proton separation energy were compared qualita-

tively to Distorted-wave Born Approximation (DWBA) calculations for different angular momentum transfer values,  $\ell$ , performed with TWOFNR [23] with the optical model parameters found in Table II.  $\ell$  values up to 3 were considered, as larger orbital angular momentum transfers are suppressed, and result in rather featureless distributions inconsistent with the data. These comparisons are shown in Figure 6. For the state at 7036(7) keV excitation energy in  $^{31}\text{S}$ , data from two previous measurements of the  $^{32}\text{S}(p,d)^{31}\text{S}$  reaction were available [13, 14]. Those data are shown with the data from the present work, in Figure 6, and found to be in good agreement. A normalization of the present differential cross section data to the measurement by Kozub et al. [13] at  $\theta_{lab} = 29^\circ$  was used to obtain the absolute cross section.

Decay protons from states above the proton separation energy in  $^{31}\text{S}$  were measured in the upstream detector in coincidence with deuterons measured in the downstream telescope. Using the calculated 2-body kinematics of the undetected recoil nucleus, the decay proton energy in the  $^{31}\text{S}$  rest frame can be calculated. The difference between the decay proton energy and the resonance energy provides the excitation energy of the final state in  $^{30}\text{P}$  populated by the decay. Figure 7 is a matrix showing the final  $^{30}\text{P}$  excitation energy deduced from the proton decay versus the  $^{31}\text{S}$  excitation energy as calculated from the deuteron produced in the original reaction. The horizontal bands represent different final states in  $^{30}\text{P}$  and moving to the right along these bands represents pro-

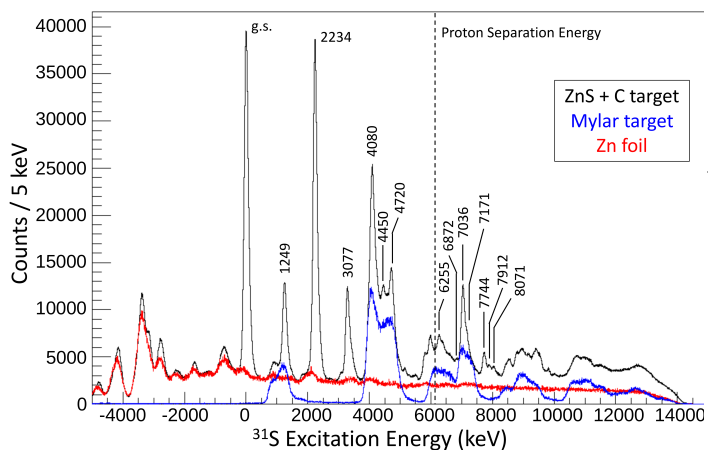


FIG. 5: (Color online) Deuteron singles spectrum corrected for the kinematics of the  $^{32}\text{S}(p,d)^{31}\text{S}$  reaction. The black histogram is the spectrum observed from the ZnS target. The ground state peak resolution is on the order of 150 keV. The blue and red histograms are the spectra observed from the mylar and zinc foils respectively, which have been normalized to the sulfur spectrum for visual clarity. Background runs on a carbon foil were also taken, but are not shown here as the peaks arising from reactions on carbon are already apparent in the mylar target data.

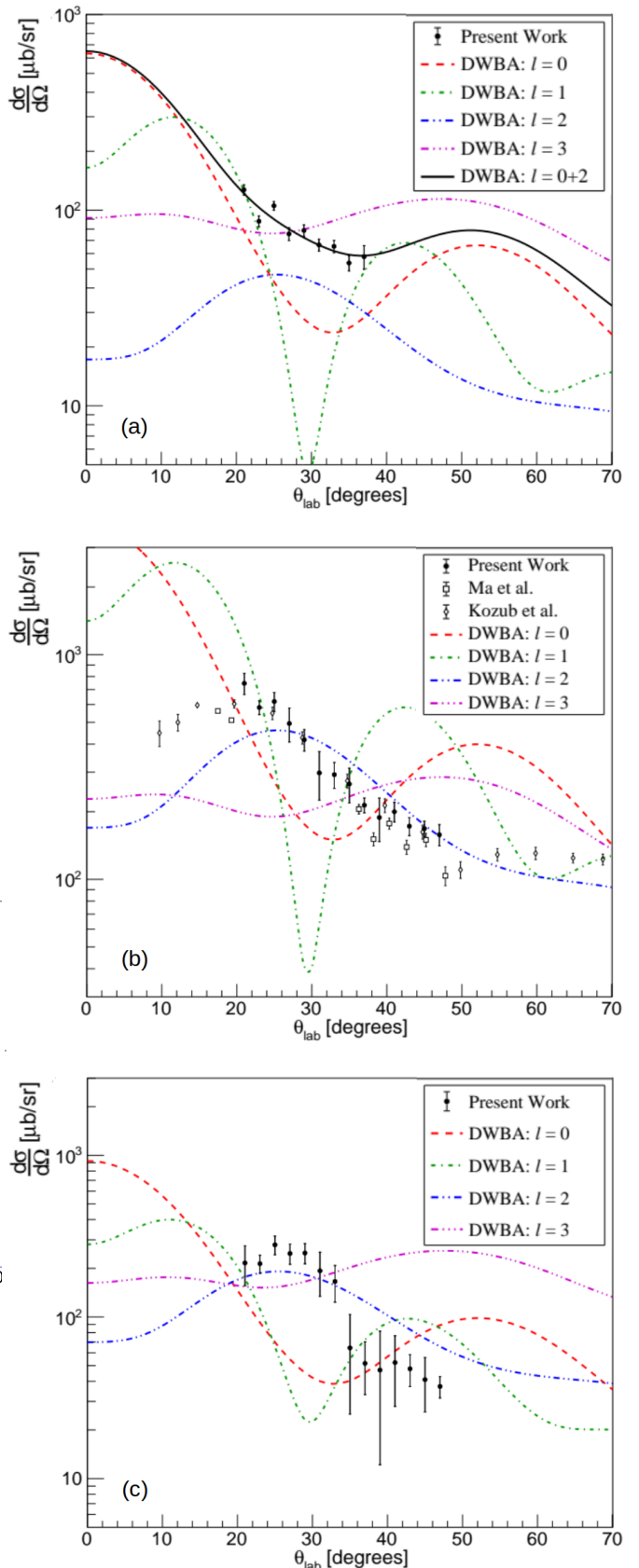


FIG. 6: (Color online) Deuteron angular distributions for the (a) 6872(6)-keV, (b) 7036(7)-keV, and (c) 7171(8)-keV states. The data from this measurement are shown as black circles. For the 7036(7)-keV state, two previous measurements reported deuteron angular distributions (Kozub et al. [13] and Ma et al. [14]) and these data are shown along side the present work. The different color curves represent DWBA calculations with

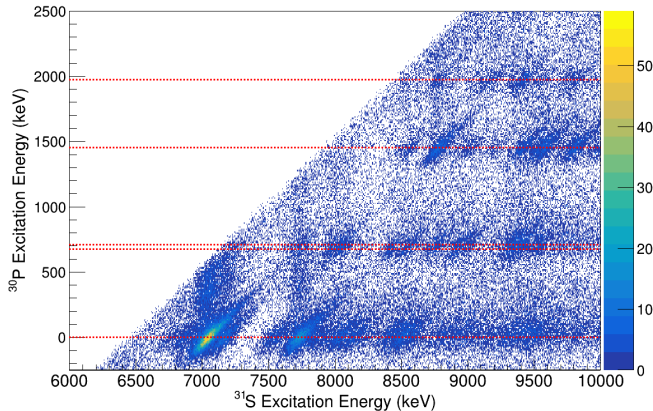


FIG. 7: (Color online) Proton decay matrix for the emission of protons from excited states in  $^{31}\text{S}$ . The excitation energy of the final state in  $^{30}\text{P}$  is shown versus the excitation energy of the initial state in  $^{31}\text{S}$ . Horizontal red dotted lines are drawn at the known excitation energies of low-lying states in  $^{30}\text{P}$ . The low-level background is due to random coincidences within the data acquisition coincidence timing window. Intensity scale (blue/dark grey to yellow/light grey) displays raw counts.

ton emission from higher energy states in  $^{31}\text{S}$ . Unfortunately, due to the efficiencies for high energy gammas, combined with small gamma branching ratios, gammas from levels above about 6.2 MeV excitation energy were not observed, and hence only proton branching ratios were extracted for these states.

The decay proton and deuteron coincidence spectra for the individual branches is generated by placing a horizontal gate around the final state of interest in  $^{30}\text{P}$  and drawing the coincident (decay-proton-gated) deuteron spectrum. Figure 8 shows the decay proton and deuteron coincidence spectra derived from Figure 7. The  $p_0$  (blue),  $p_{1,2}$  (red),  $p_3$  (green),  $p_4$  (purple) are compared to the deuteron singles spectrum (black). The coincident spectra have been scaled up by a factor of 10 for visual aid. The  $p_1$  and  $p_2$  branches have been grouped together as the final levels are only 31 keV apart and could not be individually resolved in the particle spectra. For the purposes of investigating the  $^{30}\text{P}(p, \gamma)^{31}\text{S}$  reaction rate at classical nova temperatures, only proton emission populating the ground state of  $^{30}\text{P}$  is of interest.

Broadly, the proton branching ratio is determined for each  $^{31}\text{S}$  state by dividing the number of times the level decayed (the number of proton-gated deuterons) by the number of times the level was formed (the number of deuterons), after correcting for the detection efficiencies. The efficiency corrected data from the proton decay channel to the ground state of  $^{30}\text{P}$  are plotted (cf. Fig. 9) as a function of the center-of-mass angle between the decay proton and reaction deuteron, in order to derive an angular correlation function. The detection efficiency for

decay protons was determined with a monte-carlo code in which a proton, with an energy defined by the populated  $^{31}\text{S}$  level and a direction sampled from an isotropic distribution of vectors in the rest frame of the recoiling  $^{31}\text{S}$  nucleus, was simulated. Each unique trajectory of the recoiling nucleus was considered by the corresponding deuteron trajectories available for detection in the individual segments in the telescope. The velocity of the proton in the rest frame of recoiling  $^{31}\text{S}$  nucleus was subsequently boosted into the lab frame and its trajectory was traced to determine if it intersected with a segment of the active volume of the upstream detector. The efficiency was independently calculated for each resonant state (for more detail, see Ref. [3]). For different  $^{31}\text{S}$  excitation energies, the recoiling nucleus has a different energy leading to a different detector solid angle in the  $^{31}\text{S}$  rest frame. The number of protons generated for each  $^{31}\text{S}$  trajectory was weighted by the number of detected deuterons populating that particular resonance (e.g., the number of times the resonance was formed).

Figure 9 shows the angular correlation data for the six lowest-lying observed proton decays to the  $^{30}\text{P}$  ground state. These data have been normalized by the number of times the resonance was formed. The shapes of the angular correlation data are described by a series of even-order Legendre polynomials (Equation 2), where the number of terms included in the expansion is related to the angular momentum transferred in the formation of the resonance and the subsequent decay. These data are fit with increasing orders of Equation 2 until a fit which satisfied a statistical  $p$ -value test is produced, after which no higher orders are included; this determines the minimum angular momentum of the angular correlation function. A fit was determined to have been statistically significant if the  $p$ -value was greater than 0.05, following the procedure used in a previous analysis of proton decay angular correlations as presented in Ref. [15]. The proton decay branching ratio is the result of the integration of the angular correlation fit over  $4\pi$  steradians.

$$W(\theta) = \sum_{n=0,2,4,\dots} \frac{1}{4\pi} a_n P_n(\cos \theta) \quad (2)$$

#### IV. DISCUSSION

Individual levels populated in the current work are discussed in more detail below.

**$E_x = 6255(2)$  :  $E_{\text{res}} = 124(2)$  keV :** The single direct gamma-ray transition to the ground state from a proton-unbound level in  $^{31}\text{S}$  was observed at 6254.4(16) keV, as seen in Figure 10. (As the gamma branches of particle-unbound levels are diminishingly small, the current experiment was statistics limited and did not reliably observe any peaks in the gamma spectra above this one.) This  $\gamma$  was seen in coincidence with deuterons in

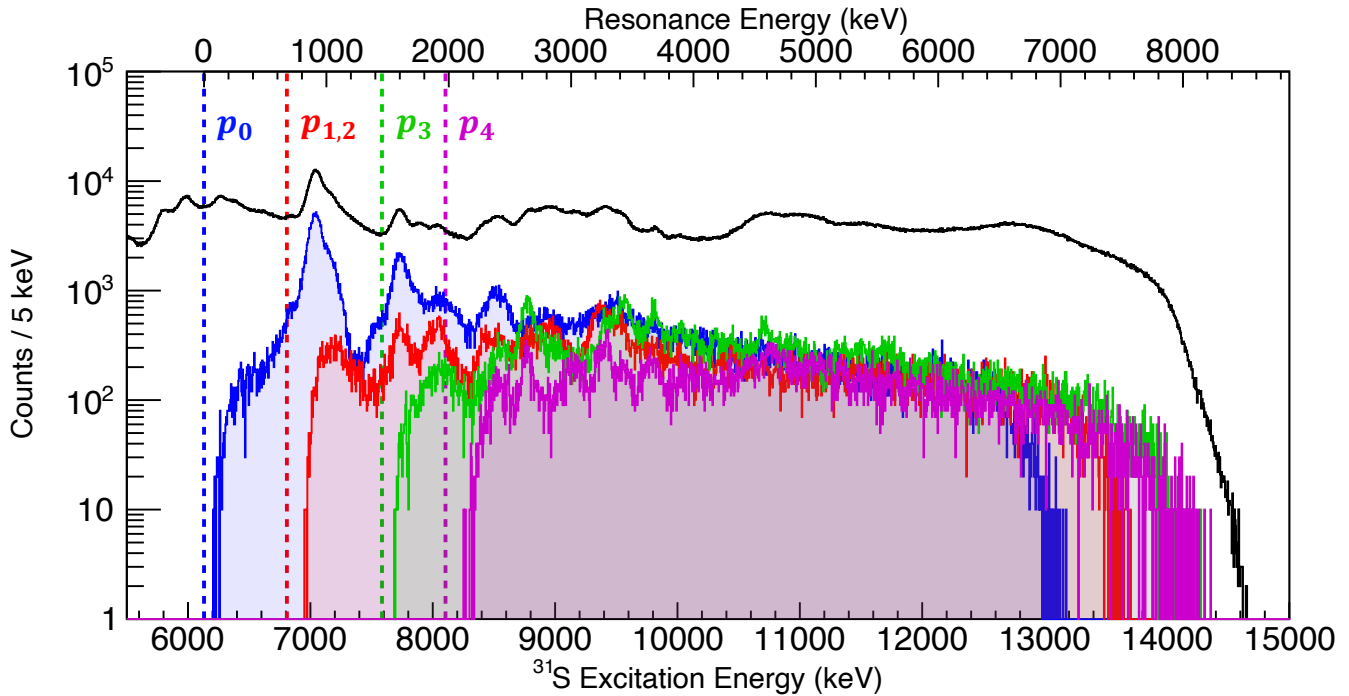


FIG. 8: (Color online) The deuteron singles spectrum (black) is compared with the deuteron-proton coincidence spectra for the  $p_0$  (blue, lowest energy threshold),  $p_{1,2}$  (red),  $p_3$  (green), and  $p_4$  (purple, highest energy threshold) proton-decay branches. All of the deuteron-proton coincidence spectra have been scaled up by a factor of 10 for visual comparison with the singles spectrum. The correspondingly-labeled dashed lines indicate the threshold for that decay channel.

the broad structure between excitation energies of 6150-6350 keV. However, the deuteron peak originating from the first excited state in carbon also fell in this region, preventing a clean angular distribution from being observed. Because of this, no gamma branching ratio could be reliably extracted from this data. Proton decays were not observed from this state.

**$E_x = 6872(6)$  :  $E_{\text{res}} = 741(6)$  keV :** A state with an excitation energy of 6872(6) keV was observed in the deuteron singles spectrum. Due to the presence of a much larger contaminant peak from the  $^{12}\text{C}(p, d)^{11}\text{C}$  reaction at higher angles, it was only possible to extract a deuteron angular distribution for this state over a limited range. The shape of the angular distribution was well matched with a mixed  $l = 0$  and  $l = 2$  transfer, with the mixing ratio being 50%, though the degree of mixing does not impact the conclusions drawn here. While the population of two distinct states cannot be ruled out, the non-observation of multiple states with similar excitation energy in previous experiments supports the conclusion that a single state was observed in this measurement. Based on this conclusion, the spin-parity of the state is constrained to  $J^\pi = (1/2 - 5/2)^+$ . A proton branching ratio of  $\Gamma_{p_0}/\Gamma = 0.53^{+0.05}_{-0.17}$  was measured in this experiment. A state with the same excitation energy and a

branching ratio of  $\Gamma_{p_0}/\Gamma = 0.37^{+0.09}_{-0.13}$  was observed by Wrede et al. [15], however they were not able to place a constraint on the spin-parity of this state. The agreement in excitation energy and proton branching ratio between the two experiments indicates the same state has been observed. With the additional information from the deuteron angular distribution a new constraint on the spin-parity of the 6872(6)-keV state has been made.

**$E_x = 7036(7)$  :  $E_{\text{res}} = 905(7)$  keV :** The deuteron angular distribution for the 7036(7)-keV state agrees well with the DWBA calculation for a  $l = 2$  transfer. Kozub et al. [13] measured a state with an excitation energy of 7050 keV and with a characteristic  $l = 2$  deuteron angular distribution. Ma et al. [14] observed a state at 7044(6) keV and found it to have a deuteron angular distribution indicating an  $l = 2$  transfer. Both authors assign this state a spin-parity of  $J^\pi = 5/2^+$ . The state measured in this work at 7036(7) keV is interpreted to be the same state observed in both Kozub et al. [13] and Ma et al. [14] based on the excitation energy and the good agreement in deuteron angular distributions.

In a measurement of the  $^{29}\text{Si}(^3\text{He}, n)^{31}\text{S}$  reaction by Davidson et al. [24], a level at 7006(25) keV was observed. This level was assigned a spin-parity of  $J^\pi = 1/2^+$  based on the neutron angular distribution being peaked at low

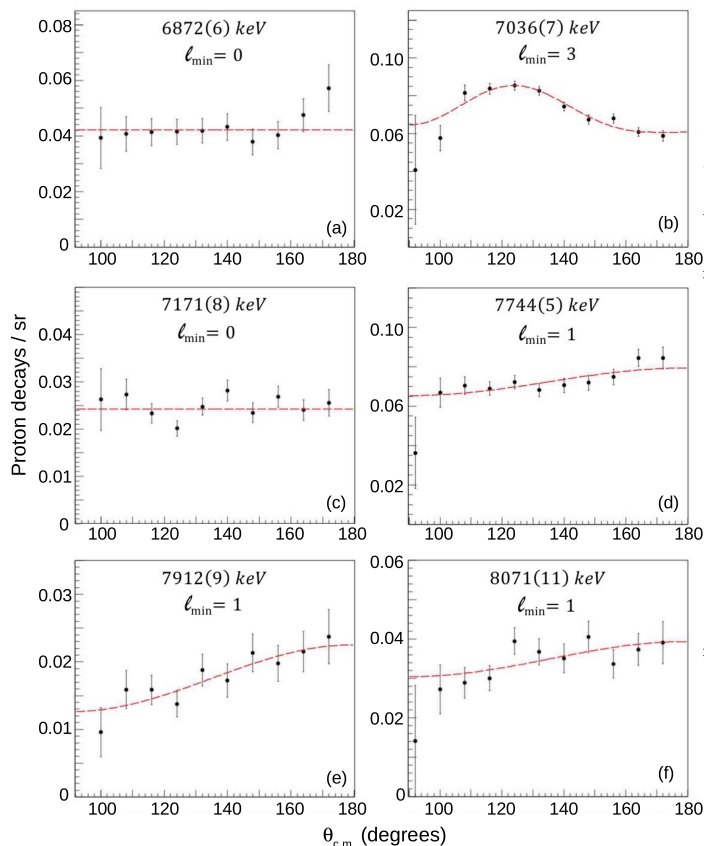


FIG. 9: (Color online) Deuteron-proton angular correlations for the six cleanly observed  $p_0$  decay branches, increasing in excitation energy from panels (a) through (f). The angular correlations, in number of decays per steradian normalized to the number of times the resonance was formed, are plotted as a function of the center of mass angle of the decay. The red dotted lines correspond to best fit to the data using Equation 2.

angles, indicating an  $l = 0$  transfer. Davidson et al. [24] reason that because the state was not observed in previous single particle transfer reactions, for which population of an isospin  $T = 3/2$  state was isospin-forbidden, this state is likely isospin  $T = 3/2$ . In addition, Davidson et al. [24] point out that shell model predictions place an isospin  $T = 3/2$  state around this region of excitation energy and that this state is expected to have a spin-parity of  $J^\pi = 1/2^+$ . Wrede et al. [15] observed a level at 7036(2) keV with a proton branching ratio of  $\Gamma_{p_0}/\Gamma = 1.05^{+0.05}_{-0.05}$ , and based on the isotropic nature of the proton decay angular correlation assigned the state a  $J^\pi = (1/2)^+$ . Using the spin-parity assignment inferred from the angular momentum of the proton decay, Wrede et al. [15] interpreted the state as being the isospin  $T = 3/2$  state that was reported at 7006(25) keV by Davidson et al. [24]. Wrede et al. [15] point out that the 7036(2)-keV state is degenerate with the  $J^\pi = 5/2^+$  state observed by both Kozub et al. [13] and Ma et al. [14], and

TABLE III: Summary of results for observed proton-emitting states. The excitation energy of the state as measured by the deuteron energy in this experiment and corresponding resonance energy are reported. The proton branching ratios from the present work are compared with the results of Wrede et al. [15].

$E_x$ (keV)	Present Work		Wrede et al. [15]	
	$J^\pi$	$E_r$ (keV)	$\Gamma_{p_0}/\Gamma$	$\Gamma_{p_0}/\Gamma$
6872(6)	$(1/2-5/2)^+$	741(6)	$0.53^{+0.05}_{-0.17}$	$0.37^{+0.09}_{-0.13}$
7036(7)	$5/2^+$	905(7)	$0.93^{+0.14}_{-0.10}$	$1.05^{+0.05}_{-0.05}$
7171(8)	$(3/2,5/2)^+$	1040(8)	$0.30^{+0.09}_{-0.06}$	$1.04^{+0.11}_{-0.63}$
7744(5)	$\geq 5/2^+{}^a$	1613(5)	$0.88^{+0.08}_{-0.04}$	$1.00^{+0.06}_{-0.06}$
7912(9)	$1/2^+{}^b$	1781(9)	$0.20^{+0.03}_{-0.03}$	$0.34^{+0.12}_{-0.29}$
8071(11)	$(1/2^+-13/2^-){}^a$	1940(11)	$0.42^{+0.08}_{-0.06}$	$1.07^{+0.22}_{-0.75}$

<sup>a</sup> Adopted from Ref. [15] <sup>b</sup> Adopted from Ref. [14]

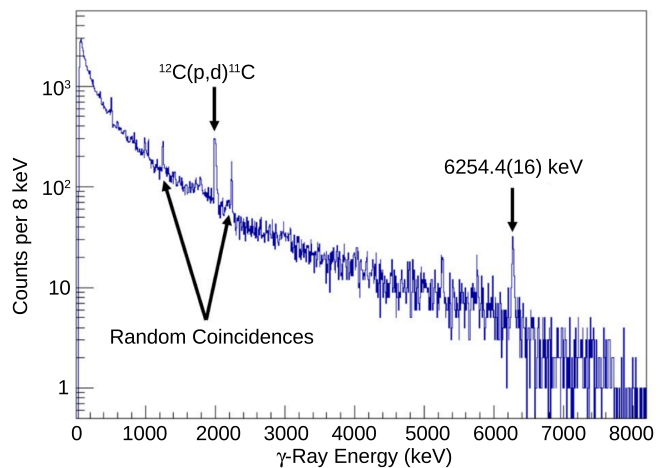


FIG. 10: (Color online) Deuteron-gated, doppler-corrected gamma spectrum showing the 6254.4(16) keV direct to ground state transition, as well as peaks arising from the contaminant  $^{12}\text{C}(p,d)^{11}\text{C}$  reaction. The deuteron gate was set to energies corresponding to  $^{31}\text{S}$  excitation energies between 6150 and 6350 keV.

therefore conclude the presence of a  $J^\pi = (1/2)^+$  state with isospin  $T = 3/2$  and a  $J^\pi = 5/2^+$  state, however, they conclude that the  $J = 5/2^+$  state was weakly populated in their measurement, and assign all of the proton decay strength to the  $J^\pi = (1/2)^+$ ,  $T = 3/2$  state.

In the more recent  $\beta$ -delayed  $\gamma$ -decay spectroscopy of Bennett *et al.* [17], a direct ground state transition corresponding to a level at 7050.0(8) is observed. This decay is assigned to be  $1/2^+ \rightarrow 1/2^+$ , identifying this as the

$T=3/2$  isospin level in the doublet. No evidence of a state around 7006 keV is observed.

In the present work, the population of a  $T = 3/2$  state is isospin-forbidden and therefore the strong population of the state reported by either Davidson et al. [24] or Bennett *et al.* [17] is unlikely. The state at 7036(7) keV had the strongest proton decay branch observed in the present work with a value of  $\Gamma_{p_0}/\Gamma = 0.93^{+0.14}_{-0.10}$ . This proton decay branching ratio value is consistent with the value measured by Wrede et al. [15] and therefore it is possible that the proton decay observed by Wrede et al. [15] was indeed from the  $J^\pi = 5/2^+$  state and not from the degenerate  $J^\pi = 1/2^+$ ,  $T = 3/2$  state. Due to the limited angular range for proton decay angular correlations in the measurement by Wrede et al. [15], it is possible that signs of the anisotropy were not observed. This present interpretation also resolves the issue of the  $p_0$  decay being isospin-forbidden and therefore expected to be small.

**$E_x = 7171(8) : E_{\text{res}} = 1040(8)$  keV :** The deuteron angular distribution for the 7171(8)-keV state suggests an  $l = 2$  transfer implying  $J^\pi = (3/2, 5/2)^+$ . Wrede et al. [15] observed two levels in the region at 7157(2) keV and 7196(2) keV. The peak observed in the present work has been interpreted as being more strongly correlated with the 7157(2)-keV state observed by Wrede et al. [15] (which may be the same as the  $5/2^+$  7149.8(9) keV level observed in Ref. [17]). While the excitation energies do not agree within  $1\sigma$ , the angular momentum reported by Wrede et al. [15] of  $J^\pi = (3/2, 5/2)^+$ , is consistent with the present measurement; the 7196(2) keV level is anticipated to be negative parity. The previously reported proton branching ratio of  $\Gamma_{p_0}/\Gamma = 1.04^{+0.11}_{-0.63}$  has a very large uncertainty, and the value measured in this work, while just outside of that uncertainty, has a greatly reduced uncertainty. The nature of the large discrepancy in proton branching ratio between the current and previous works is unclear.

**$E_x = 7744(5) : E_{\text{res}} = 1613(5)$  keV :** The limited statistics in the deuteron spectrum did not allow for a comparison with DWBA calculations to infer the transferred angular momentum. A state in  $^{31}\text{S}$  with an excitation energy of 7744(3) keV was reported by Wrede et al. [15]. The branching ratio measured in that experiment is consistent with the value measured in this work. Due to the good agreement in excitation energy and branching ratio this state has been interpreted as the same observed by Wrede et al. [15].

**$E_x = 7912(9) : E_{\text{res}} = 1781(9)$  keV :** A state at 7912(5) keV was reported by Ma et al. [14], and found to have a deuteron angular distribution consistent with an  $l = 0$  transfer. Wrede et al. [15] observed a state with an excitation energy of 7905(3) keV. The state measured in this work with an excitation energy of 7912(9) keV is interpreted as the same state observed by Ma et al. [14] and Wrede et al. [15]. The uncertainty in  $\Gamma_{p_0}/\Gamma$  for this state has been reduced significantly.

**$E_x = 8071(11) : E_{\text{res}} = 1940(11)$  keV :** This state was weakly populated and therefore there were not enough statistics at individual angles to extract a deuteron angular distribution. A state with an excitation energy of 8071(11) keV was also reported by Wrede et al. [15]. The excitation energy and branching ratio reported by both measurements agree within uncertainty. The present work was able to significantly reduce the uncertainty in  $\Gamma_{p_0}/\Gamma$  for this state.

## V. CONCLUSION

The  $^{30}\text{P}(p, \gamma)^{31}\text{S}$  reaction rate is currently one of the largest remaining source of uncertainty in ONe nova nucleosynthesis, and this uncertainty inhibits the usefulness of key nova observables such as spectroscopy of ejecta and presolar grain analysis. The  $^{32}\text{S}(p, d)^{31}\text{S}^*(p)^{30}\text{P}$  reaction has been measured to obtain information about the resonant states that are important for constraining the  $^{30}\text{P}(p, \gamma)^{31}\text{S}$  reaction rate. A summary of the measured excitation energies and decay proton branching ratios is presented in Table III. This experiment was able to reduce the uncertainty in proton-decay branching ratios for several states at higher excitation energies.

We conclude that a previous measurement by Wrede et al. [15] may have incorrectly assigned the strong  $p_0$  decay branch of a state at 7036(2) keV to a  $T = 3/2$ ,  $J^\pi = 1/2^+$  level previously placed at 7006(25) keV [24] or, more likely, 7050.0(8) keV [17]. The current work observed a similarly strong  $p_0$  from a state with an excitation energy of 7036(7) keV and place it as the previously identified  $T = 1/2$ ,  $J^\pi = 5/2^+$  [13, 14].

The resonances observed in this experiment were all higher in energy than the resonances that dominate the reaction rate at classical nova temperatures; because of this, we do not provide a recommended  $^{30}\text{P}(p, \gamma)^{31}\text{S}$  reaction rate. In addition, there were some difficulties in resolving states in the region of interest and contributions from  $(p, d)$  reactions on the other nuclei present in the target, limiting the range of the derived angular distributions. Despite these challenges, in these results, several assignments for states above the proton separation energy in  $^{31}\text{S}$  were confirmed and the uncertainties for some proton decay branching ratios were reduced. For the lowest-energy resonances, alternative techniques such as measurements with gas-filled detectors [18] and mirror-symmetry spectroscopy [25, 26] may provide the critical branching ratios, taking advantage of the spin and parity assignments and other structure information derived in this and similar work.

The novel analysis techniques for proton decay measurements developed in this work enables the extension of these types of measurements to large solid angle charged-particle arrays. A future measurement utilizing a different target and reaction to populate states in  $^{31}\text{S}$  would benefit from the work performed here in developing analysis techniques for use in proton decay measurements

with large solid-angle charged-particle arrays. In addition, the extension of this analysis to the  $p_{1,2}$ ,  $p_3$ , and  $p_4$  branches is possible with data obtained in this experiment. Future high-statistics experiments should provide sufficient data to utilize particle-gamma or particle-gamma-gamma coincidences to further constrain level energies and branching ratios critical to our understanding of explosive nucleosynthesis.

## ACKNOWLEDGMENTS

This material is based upon work supported by the U.S. DOE, Office of Science, Office of Nuclear Physics under contracts DE-FG02-96ER40983 (UTK), DE-AC05-00OR22725 (ORNL), DE-NA-0003780 (Notre Dame), DE-NA0002132 (Rutgers), DE-FG03-93ER40773 (TAMU), and DE-NA-0003841 (CENTAUR). This work was performed under the auspices of the U.S. DOE by Lawrence Livermore National Laboratory under Contract DE-AC52-07NA27344. Additional support came from The Welch Foundation, the NSF under PHY-1430152 (JINA-CEE) and PHY-1812316 (Rutgers), and the Laboratory Directed Research and Development (LDRD) Program of ORNL.

- 
- [1] J. José, A. Coc, and M. Hernanz, *The Astrophysical Journal* **560**, 897 (2001).
- [2] S. Starrfield, C. Iliadis, and W. R. Hix, *Publications of the Astronomical Society of the Pacific* **128**, 051001 (2016).
- [3] S. Burcher, Ph.D. Dissertation, University of Tennessee Knoxville (2019).
- [4] S. Amari, X. Gao, L. R. Nittler, E. Zinner, J. Jose, M. Hernanz, and R. S. Lewis, *The Astrophysical Journal* **551**, 1065 (2001).
- [5] J. Jose, M. Hernanz, S. Amari, K. Lodders, and E. Zinner, *The Astrophysical Journal* **612**, 414 (2004).
- [6] L. N. Downen, C. Iliadis, J. José, and S. Starrfield, *The Astrophysical Journal* **762**, 105 (2013).
- [7] K. J. Kelly, C. Iliadis, L. Downen, J. José, and A. Champagne, *The Astrophysical Journal* **777**, 130 (2013).
- [8] C. Iliadis, A. Champagne, J. Jose, S. Starrfield, and P. Tupper, *The Astrophysical Journal Supplement Series* **142**, 105 (2002).
- [9] T. Rauscher and F.-K. Thielemann, *Atomic Data and Nuclear Data Tables* **75**, 1 (2000).
- [10] D. G. Jenkins, A. Meadowcroft, C. J. Lister, M. P. Carpenter, P. Chowdhury, N. J. Hammond, R. V. F. Janssens, T. L. Khoo, T. Lauritsen, D. Seweryniak, T. Davinson, P. J. Woods, A. Jokinen, H. Penttila, G. Martínez-Pinedo, and J. José, *Phys. Rev. C* **73**, 065802 (2006).
- [11] D. T. Doherty, G. Lotay, P. J. Woods, D. Seweryniak, M. P. Carpenter, C. J. Chiara, H. M. David, R. V. F. Janssens, L. Trache, and S. Zhu, *Phys. Rev. Lett.* **108**, 262502 (2012).
- [12] A. Kankainen, P. Woods, H. Schatz, T. Poxon-Pearson, D. Doherty, V. Bader, T. Baugher, D. Bazin, B. Brown, J. Browne, A. Estrade, A. Gade, J. José, A. Kontos, C. Langer, G. Lotay, Z. Meisel, F. Montes, S. Noji, F. Nunes, G. Perdikakis, J. Pereira, F. Recchia, T. Redpath, R. Stroberg, M. Scott, D. Seweryniak, J. Stevens, D. Weisshaar, K. Wimmer, and R. Zegers, *Physics Letters B* **769**, 549 (2017).
- [13] R. L. Kozub, *Physical Review* **172**, 1078 (1968).
- [14] Z. Ma, D. W. Bardayan, J. C. Blackmon, R. P. Fitzgerald, M. W. Guidry, W. R. Hix, K. L. Jones, R. L. Kozub, R. J. Livesay, M. S. Smith, J. S. Thomas, and D. W. Visser, *Phys. Rev. C* **76**, 015803 (2007).
- [15] C. Wrede, J. A. Caggiano, J. A. Clark, C. M. Deibel, A. Parikh, and P. D. Parker, *Phys. Rev. C* **79**, 045803 (2009).
- [16] M. B. Bennett, C. Wrede, B. A. Brown, S. N. Liddick, D. Pérez-Loureiro, D. W. Bardayan, A. A. Chen, K. A. Chipps, C. Fry, B. E. Glassman, C. Langer, N. R. Larson, E. I. McNeice, Z. Meisel, W. Ong, P. D. O'Malley, S. D. Pain, C. J. Prokop, H. Schatz, S. B. Schwartz, S. Suchyta, P. Thompson, M. Walters, and X. Xu, *Phys. Rev. Lett.* **116**, 102502 (2016).
- [17] M. B. Bennett, C. Wrede, S. N. Liddick, D. Pérez-Loureiro, D. W. Bardayan, B. A. Brown, A. A. Chen, K. A. Chipps, C. Fry, B. E. Glassman, C. Langer, N. R. Larson, E. I. McNeice, Z. Meisel, W. Ong, P. D. O'Malley, S. D. Pain, C. J. Prokop, H. Schatz, S. B. Schwartz, S. Suchyta, P. Thompson, M. Walters, and X. Xu, *Phys. Rev. C* **97**, 065803 (2018).
- [18] T. Budner *et al.*, submitted to *Phys. Rev. Lett.* (2021).
- [19] C. Wrede, *AIP Advances* **4**, 041004 (2014), <https://doi.org/10.1063/1.4864193>.
- [20] R. Hughes, J. Burke, R. Casperson, S. Ota, S. Fisher, J. Parker, C. Beausang, M. Dag, P. Humby, J. Koglin, E. McCleskey, A. McIntosh, A. Saastamoinen, A. Tamashiro, E. Wilson, and T. Wu, *Nuclear Instruments and Methods in Physics Research Section A: Accelerators, Spectrometers, Detectors and Associated Equipment* **856**, 47 (2017).
- [21] <http://www.micronsemiconductor.co.uk> (2022).
- [22] A. A. Cowley, G. Heymann, R. L. Keizer, and M. J. Scott, *Nuclear Physics A* **86**, 363 (1966).
- [23] M. Toyama, M. Igarashi, and N. Kishida, "TWOFRN Computer Code, Unpublished."
- [24] J. M. Davidson, D. A. Hutcheon, D. R. Gill, T. Taylor, D. M. Sheppard, and W. C. Olsen, *Nuclear Physics A* **240**, 253 (1975).
- [25] S. D. Pain, D. W. Bardayan, J. C. Blackmon, S. M. Brown, K. Y. Chae, K. A. Chipps, J. A. Cizewski, K. L. Jones, R. L. Kozub, J. F. Liang, C. Matei, M. Matos, B. H. Moazen, C. D. Nesaraja, J. Okołowicz, P. D. O'Malley, W. A. Peters, S. T. Pittman, M. Płoszajczak, K. T. Schmitt, J. F. Shriner, D. Shapira, M. S. Smith, D. W. Stracener, and G. L. Wilson, *Phys. Rev. Lett.*

114, 212501 (2015).

[26] R. Ghimire *et al.*, APS Division of Nuclear Physics Meeting (2020).